Semiconductor moiré materials

Kin Fai Mak[1-3] and Jie Shan[1-3]

[1]Laboratory of Atomic and Solid State Physics, Cornell University, Ithaca, NY, USA
[2]School of Applied and Engineering Physics, Cornell University, Ithaca, NY, USA
[3]Kavli Institute at Cornell for Nanoscale Science, Ithaca, NY, USA

Email: kinfai.mak@cornell.edu; jie.shan@cornell.edu

Moiré materials have emerged as a new platform for exploring strong electronic correlation and topological physics. Here we review the recent progress in semiconductor moiré materials, with a particular focus on transition metal dichalcogenide (TMD) semiconductors. Following a brief overview of the general features of this class of materials, we will discuss recent theoretical and experimental progress on the studies of Hubbard physics, Kane-Mele-Hubbard physics and moiré exciton physics. We will also provide an outlook on future opportunities and challenges in TMD and other semiconductor moiré materials.

Introduction

Arguably, one of the most exciting developments in condensed matter physics in the last few years is the discovery of moiré materials [1-3]. These materials form when two layers of van der Waals materials stack on top of each other with either a small twist angle or a lattice mismatch. A moiré superlattice structure emerges as a result of the interference in the atomic lattice structures of the constituent materials (Fig. 1a). The periodicity of the superlattice structure, the moiré period a_M, is many times bigger than the atomic lattice constant a. This difference in length scales allows the separation of the low-energy physics (set by the scale a_M) from the high-energy physics (set by the scale a) [4]. Electrons in moiré materials can thus be treated as moving in a smooth periodic potential (Fig. 1b); the atomic lattice structure of the constituent materials can be discarded as far as low-energy physics is concerned. Bloch's theorem applies to the moiré mini-Brillouin zone associated with the superlattice and moiré flat bands emerge (Fig. 1c).

The emergence of the new length scale a_M and the associated low-energy physics endows moiré materials a highly controllable quantum system. The new moiré atomic density $\sim a_M^{-2}$ is about three orders of magnitude smaller than the original atomic density $\sim a^{-2}$. The maximum doping density in a typical field-effect device is up to ~ 1 % of a^{-2} before the gate dielectrics break down. Electrostatic gating can therefore fill many electrons in each artificial moiré atom (with size $\sim a_M$, Fig. 1b). This is significant because every integer filling of electrons is analogous to a different chemical element in real materials. In addition to controls of electron filling, the moiré flat bands, which have bandwidth about one to two orders of magnitude smaller than that of real materials, are also highly susceptible to external stimulus, such as external electric fields [3, 5, 6] and pressure [7]. In general, terms in a many-body moiré Hamiltonian are continuously tunable.

The emergence of the moiré length scale also makes moiré materials a unique platform for studies of strong correlation physics [8-10]. Because the on-site Coulomb repulsion between two electrons in the same moiré site scales as $U \propto a_M^{-1/2}$ (Ref. [11]) and the moiré bandwidth (or the kinetic energy in 2D for massive electrons) scales as $W \propto a_M^{-2}$, U completely dominates over W for large moiré periods. In general, electrons in moiré materials with flat bands are strongly correlated and the degree of electronic correlation is tunable by changing the scale a_M.

Experimental studies on moiré materials started soon after the discovery of graphene [12-14]. Scanning tunneling microscopy (STM) studies have directly observed the formation of moiré patterns and enhanced density of states in small-angle twisted bilayer graphene [15]. Theoretical investigations of the electronic properties followed almost immediately [4, 16, 17]. Intriguingly, moiré flat bands that can substantially enhance electronic correlations were predicted at specific "magic" angles. The magic of these flat band systems was not revealed until the discovery of superconductivity near correlated insulating states in magic-angle twisted bilayer graphene [2, 18]. The result has attracted tremendous attention in the physics community ever since.

In this review we will focus on semiconductor moiré materials (readers interested in graphene moiré materials please refer to Ref. [9, 10]). Compared to twisted bilayer graphene built on Dirac massless electrons (Table I), semiconductor moiré materials built on massive electrons have two important differences. First, there is no magic angle condition for the formation of flat bands [19-21]. Because of the energy gap in 2D semiconductors, moiré flat bands can be formed in a continuous range of twist angles. Second, the flat bands in semiconductor moiré materials (both topological and non-topological) admit a local tight-binding description in the moiré lattice [19, 20]. This is in general not possible in twisted bilayer graphene because of Wannier obstruction [22].

Among all of the 2D semiconductors, we will further limit our focus to the family of transition metal dichalcogenide (TMD) semiconductors, where significant progress has been made in recent years. Monolayer TMDs are direct band gap semiconductors [23, 24] with relatively low disorder densities ($\lesssim 10^{11}$ cm^{-2}) for electron transport studies [25]. They have unique spin-valley locked electronic band structure and valley-dependent optical selection rules [26] that form the basis for optical probes of magnetism. (See Ref. [27, 28] for a review on the basic properties of monolayer TMDs.) The lattice mismatch in the family of TMDs (varies from ~ 0 % to ~ 13 %) and the tunable twist angle allow the formation of moiré lattices with a wide range of moiré density (~ 10^{12} – 10^{13} cm^{-2}). Moreover, hetero-bilayers built on lattice-mismatched monolayers are generally insensitive to twist angle disorders compared to homo-bilayers (Fig. 1d). For these reasons, robust strong correlation and topological physics as well as their interplay have been demonstrated; robust moiré exciton physics has also been reported. We will review these recent developments below.

Moiré superlattice structure

TMD moiré materials form by stacking two identical monolayers on top of each other with a small twist angle θ (homo-bilayer) [29-31] or by stacking two different monolayers with a lattice mismatch δ (hetero-bilayer) [32-37]. A hexagonal superlattice structure is formed; the moiré period in the former is $a_M \approx \frac{a}{\theta}$ and the latter is $a_M \approx \frac{a}{\sqrt{\delta^2+\theta^2}}$ (Fig. 1d). The typical moiré period is $a_M \sim 10\text{nm} \gg a \sim 1\text{Å}$. There are two different stacking structures for each case: AA- and AB-stacking. For AA-stacking, there are three high-symmetry sites in the superlattice (Fig. 1a): the MX site, in which the transition metal atom M (= Mo, W) in the top layer lays directly on top of the two chalcogen atoms X (= S, Se, Te) in the bottom layer; the XM site, the inverse of the MX site; and the MM (or XX) site with M (X) in one layer directly on top of M (X) in the other. The high symmetry sites in AB-stacking are different (Fig. 1b). These include the MX site (this is the stacking structure of the natural bilayer material) and the MM and XX sites.

The fabrications of homo- and hetero-bilayer moiré structures are quite different. The tear-and-stack technique is employed for homo-bilayers [38-40]. A single TMD monolayer obtained from mechanical exfoliation is torn apart into two halves, which are then re-stacked on top of each other with a controllable twist angle θ. The procedure is almost identical to that for twisted bilayer graphene. In contrast, two different TMD monolayers obtained from separate exfoliations are involved in the fabrication of hetero-bilayers. Predetermination of the crystal axis for each monolayer is required in order to create angle-aligned hetero-bilayers. This is often achieved by polarization- and angle-resolved optical second harmonic generation (SHG) spectroscopy [32-34]. Typical angle alignment accuracy is about $\pm 0.5°$, which is much less accurate compared to homo-bilayers. However, this hardly matters because the moiré period of hetero-bilayers $a_M \approx \frac{a}{\delta}$ is dominated by the lattice mismatch $\delta \gg \theta$ (Fig. 1d). The insensitivity of the moiré lattice on twist angle (and therefore twist angle disorders) is a major advantage of hetero-bilayers with larger lattice mismatch $\delta \gg \theta$.

The superlattice structure of TMD moiré materials has been characterized by transmission electron microscopy (TEM) [34, 41], scanning tunneling microscopy (STM) [30, 42], piezoresponse force microscopy (PFM) [43] and density functional theory (DFT) calculations [5, 42, 44]. The structure is far from the idealized rigid structure without lattice distortion in the constituent monolayers. First, there is lattice reconstruction within each monolayer to maximize the area of the most stable stacking structure in each moiré unit cell. This creates a spatially periodic strain modulation within each monolayer, which modulates the TMD band gap and contributes to the total periodic moiré potential [42]. Second, there is unintentional relative strain between the constituent monolayers from fabrications; it distorts the perfect hexagonal superlattice structure. The unintentional strain can vary randomly over the sample and acts as a disorder potential. Third, unintentional twist angle variations randomly distributed over the sample creates random variations in the moiré period over a length scale smooth compared to a_M and acts as another source of disorder potential. Such disorder effect is particular important in homo-bilayers [43], in which a_M is sensitive to θ. Finally, large-scale reconstructions into random patches of the stable stacking structure and/or stripy patterns can occur in samples with

large moiré period, such as homo-bilayers with small twist angle [43]. The entire moiré superlattice structure can be lost in extreme cases.

Semiconductor moiré flat bands

A good starting point to understand the electronic band structure of TMD and other semiconductor moiré materials is the continuum model [4, 19, 20]. In the limit $a_M \gg a$, the high-energy physics set by the atomic scale is well separated from the low-energy physics set by the moiré length scale. To a good approximation, electrons in TMD moiré materials can be treated as particles with an effective band mass m of the constituent TMD monolayers moving in a smooth periodic moiré potential V_M (Fig. 1b). This picture gives a moiré Hamiltonian $H_M = \frac{p^2}{2m} + V_M$. Here p is the quasi-momentum operator and V_M can be approximated by a Fourier expansion of harmonics associated to different moiré reciprocal lattice vectors [4, 19, 20]. Application of the Bloch's theorem leads to a series of flat bands in the moiré mini-Brillouin zone (Fig. 1c).

The spatial dependence of V_M can be obtained by calculating the dependence of the monolayer TMD band edge energy on the relative atomic displacement between the two TMD layers using DFT methods [19, 20, 45]. Because the relative atomic displacement varies smoothly in the moiré length scale, such band edge modulation corresponds to the moiré potential. The monolayers are treated as rigid in this approximation; only the contribution to V_M from spatially modulated interlayer hopping is taken into account. Another method to calculate V_M is to first obtain the moiré flat bands using large-scale DFT calculations that include lattice relaxations in the superlattice structure [5, 21, 42, 44]; the moiré band dispersion is then fit to a continuum model to obtain V_M (Ref. [44, 46]). Both contributions to V_M from spatially modulated interlayer hopping and periodic intralayer strain from lattice relaxations are taken into account in this method. The relaxed structure is, however, sensitive to the choice of van der Waals functionals.

Hubbard model physics

For angle-aligned TMD hetero-bilayers and twisted TMD homo-bilayers with layer asymmetry (e.g. under a vertical electric field), the layer degeneracy of the electronic bands is lifted; the intrinsic Ising spin-orbit coupling in the constituent TMD monolayers lifts the spin degeneracy within a single electronic valley [26-28]. As a result, only a two-fold valley degree of freedom with approximate SU(2) symmetry remains for the first moiré conduction/valence band [11, 19]. This isolated flat band can be mapped to a tight-binding model in a triangular lattice with a nearest neighbor hopping term t [19]. The effect of electronic Coulomb interactions can be included as an on-site Coulomb repulsion U and an extended Coulomb repulsion V (Ref. [19, 45, 47, 48]). The system effectively realizes a single-band extended Hubbard model on a triangular lattice [19, 45, 47-49] (Fig. 1a, b). For AB-stacked homo-bilayers, in which interlayer hopping is spin-forbidden, a two-band Hubbard model with approximate SU(4) symmetry in the valley-layer space can also be realized [20, 50].

The hopping term can be estimated as $t = \frac{W}{9} \sim \frac{\hbar^2\pi^2}{9ma_M^2} \sim 1-5$ meV for a typical band mass $m \sim 0.5m_0$ in TMDs [51] (m_0 is the free electron mass) and for typical moiré period $a_M \sim 5-10$ nm ($\hbar$ is the Planck's constant); the factor 9 comes from the triangular lattice structure. The on-site Coulomb term can be estimated as $U \sim \frac{e^2}{4\pi\epsilon\epsilon_0 a_W} \sim 100-200$ meV for a typical size of the localized Wannier orbital $a_W \sim 2$ nm [19] and the dielectric constant of hBN $\epsilon \sim 4-5$ (Ref. [52]) (e and ϵ_0 denote the electron charge and the vacuum permittivity, respectively). The extended Coulomb term V can be estimated based on the Coulomb potential and the triangular lattice structure; for instance, the nearest neighbor Coulomb repulsion is $V_1 \sim \frac{e^2}{4\pi\epsilon\epsilon_0 a_M} \sim 50-100$ meV. We can see from such estimates that TMD moiré materials simulate Hubbard model physics in the strong correlation limit $U > V > W$. Experimentally, V can be effectively tuned by the sample-gate distance due to screening [53-55]; t can be tuned by either the sample twist angle [19, 29, 45, 47] or a vertical electric field that controls the moiré potential depth [5, 6]; and the average filling factor of electrons/holes per moiré unit cell ν is tuned by electrostatic gating. Below we summarize recent experimental developments.

Mott insulator. The on-site Coulomb term U dominates the physics at filling factor $\nu = 1$ (corresponding to half-band-filling). In the strong correlation limit $U > W$, a robust insulating state has been observed by multiple experimental groups on various TMD moiré systems (Fig. 2a), which include angle-aligned WSe_2/WS_2 (Ref. [32, 33]), $MoSe_2/WS_2$ (Ref. [53]) and $MoTe_2/WSe_2$ (Ref. [5, 56]), and twisted WSe_2 (Ref. [6, 29]) and $MoSe_2$ (Ref. [31]). Such insulating state is not expected from the single-particle band theory. It is consistent with the emergence of a Mott insulator [57] if the single-particle moiré bands are far apart compared to U or a charge-transfer insulator in the opposite limit [11]. The insulating state emerges as an attempt of the system to minimize the on-site Coulomb repulsion by localization of the charge carriers. The charge degree of freedom is frozen; the low-energy physics is governed by the collective spin excitations from the local magnetic moments [58]. The magnetic ground state is expected to be 120-degree Néel order [45] (Fig. 2a). The emergence of local magnetic moments has been verified by temperature dependent magnetic circular dichroism (MCD) measurements [32]. This is possible thanks to the spin-valley locked band structure and the valley-dependent optical selection rules in monolayer TMDs [26-28]; the MCD signal is directly proportional to the sample magnetization. A Curie-Weiss behavior for the magnetic susceptibility with a negative Curie-Weiss temperature is observed (Fig. 2b). The result is consistent with the expected Anderson superexchange interaction between local magnetic moments in a Mott insulator [58]. The far apart local magnetic moments (separated by $a_M \sim 5-10$ nm) give a weak superexchange energy scale about 1-30 K (Ref. [5, 32]).

Continuous Mott transition. Whereas the system at $\nu = 1$ is Mott insulator in the $U \gg W$ limit, it is a Fermi liquid in the opposite limit $U \ll W$. A transition between the two states of matter is expected to happen at $U \sim W$ (Ref. [57, 58]). Such metal-insulator transition is often driven first-order and accompanied by simultaneous magnetic, structural and other forms of phase transitions [58]. However, the geometrically frustrated Mott insulator in a triangular lattice and the reduced dimensionality in TMD moiré systems can quench these

undesired phase transitions and favor an unusual continuous transition from a non-magnetic Mott insulator to a Fermi liquid without symmetry breaking, known as the continuous Mott transition [59-61]. The non-magnetic Mott insulator near the transition has also been predicted to be some forms of quantum spin liquids [59-64].

The possibility to realize bandwidth-tuned Mott transitions in TMD moiré materials has been discussed by Ref. [65, 66]. Two recent experiments on two different TMD moiré systems, twisted WSe_2 (Ref. [6]) and AA-stacked $MoTe_2/WSe_2$ hetero-bilayers [5], have reported a continuous metal-insulator transition at a fixed filling factor $\nu = 1$ induced by electric field tuning of the moiré bandwidth W (Fig, 2d, e). The application of a vertical electric field shifts the moiré band alignment, modifies the interlayer hopping strength and the moiré potential depth, and therefore changes W predominantly. It effectively tunes the interaction strength measured by U/W. Specifically, the transport data in AA-stacked $MoTe_2/WSe_2$ hetero-bilayers have shown a continuously vanishing charge gap as the critical point is approached from the insulating side as well as a diverging quasiparticle effective mass and an abrupt disappearance of the entire Fermi surface from the metallic side. MCD measurements have further shown a smooth evolution of the magnetic susceptibility across the critical point and the absence of long-range magnetic ordering down to ~ 5 % of the Curie-Weiss temperature. The transport data in twisted WSe_2 have also suggested the emergence of a linear-in-temperature resistivity near the critical point. Although many of these observations, especially in AA-stacked $MoTe_2/WSe_2$ hetero-bilayers, are consistent with the universal critical theory of a continuous Mott transition [59, 67, 68], recent theoretical studies have pointed out the importance of Coulomb disorders and percolation transport near the metal-insulator transition [69, 70]. The effects of disorder and the nature of the magnetic ground state near the transition [68] and its relevance to quantum spin liquids deserve further in-depth investigations.

Charge-ordered states. Whereas the on-site U term dominates the physics at $\nu = 1$, the extended Coulomb interaction V becomes important away from $\nu = 1$. In the strong correlation limit $U > V > W$, the minimization of the extended Coulomb repulsion between electrons drives the spontaneous formation of incompressible charge-ordered states at commensurate fractional filling factors [47, 48, 71, 72]. An abundance of such charge-ordered states have been observed by multiple experimental groups using different experimental techniques and on different TMD moiré systems (Fig. 2a), including angle-aligned WSe_2/WS_2 (Ref. [33, 52, 73-75]), $MoSe_2/WS_2$ (Ref. [53]) and $MoTe_2/WSe_2$ (Ref. [5, 56]). The experimental techniques include optical detection of compressibility [33], direct compressibility measurement [53], Rydberg state sensing of dielectric function [52], microwave impedance microscopy [73] and photoluminescence (PL) spectroscopy [75]. In addition, a recent STM study based on imaging the local chemical potential of a graphene gate electrostatically coupled to the charge-ordered states has directly obtained the charge ordering patterns [74] (Fig. 2c). Here the charge-ordered states directly imprint the periodic electrostatic potential onto the nearby graphene gate and modulate the local chemical potential of the graphene.

In addition to charge-ordered states that preserve the rotational symmetry of the system (often referred to as generalized Wigner crystals), the competing short-range and long-range Coulomb interactions between electrons can drive the formation of stripe phases that spontaneously break the rotational symmetry [76-78] (Fig. 2a). The stripe phases can be further divided into stripe crystal phases at commensurate fractional fillings and electronic liquid crystals at incommensurate fillings [78, 79]. The stripe crystal phases are incompressible and have been directly detected by optical birefringence imaging [80] and STM [74]. The electronic liquid crystals (e.g. smectic and nematic phases) are compressible and have been observed by combined optical birefringence and compressibility measurements [80].

Finally, we note that similar to the Mott transition discussed above a bandwidth-tuned metal-insulator transition from an incompressible charge-ordered state to a Fermi liquid at fixed commensurate fractional filling is expected at $V \sim W$ (Ref. [81, 82]). This is analogous to the famous Wigner transition, i.e. quantum melting of a Wigner crystal to a Fermi liquid [83]. Signatures of such transition have been reported by Ref. [5] (Supplementary Materials). More in-depth studies are required to understand the nature of this quantum phase transition. We summarize in Fig. 3a the experimental Hubbard phase diagram obtained from TMD moiré materials to date.

Kane-Mele-Hubbard physics

AA-stacked homo-bilayers. Whereas the Hubbard physics discussed above comes from an isolated, non-topological moiré band [19], intertwining two TMD moiré bands through complex hopping can introduce non-trivial band topology [20]. This has been first predicted in AA-stacked twisted TMD homo-bilayers [20], in which spin-preserved interlayer hopping is allowed. The moiré Hamiltonian has two components, one for each monolayer; it contains the kinetic energy and the intralayer moiré potential for each layer and a complex interlayer moiré potential that can intertwine two layer-copies of moiré bands. The interlayer hopping splits the otherwise layer-degenerate moiré valence bands into topological bands with non-zero valley-resolved Chern numbers (Fig. 4a, b). The first two topological moiré bands can be mapped to a tight-binding model on a honeycomb lattice (Fig. 4a), which includes a nearest neighbor *interlayer* hopping between the non-equivalent MX and XM sublattice sites, a next nearest neighbor *intralayer* hopping within each sublattice, and an *interlayer* sublattice potential difference continuously tunable by a vertical electric field. The next nearest neighbor hopping term also carries a bond- and spin-dependent phase shift that gives rise to an effective Ising spin-orbit coupling. The model is therefore equivalent to the Kane-Mele model [84]. A transition to non-topological bands is expected at sufficiently large electric fields [20, 46].

Including the on-site Coulomb repulsion U in the honeycomb lattice further gives the Kane-Mele-Hubbard Hamiltonian [85]. The presence of both electronic correlation and non-trivial band topology in this model is expected to support a wealth of exotic electronic states of matter [86]. Depending on the relative strength of the different terms in the Hamiltonian, quantum spin Hall insulator, antiferromagnetic insulator, antiferromagnetic Chern insulator and quantum spin liquids have been predicted at $\nu = 2$ (Ref. [85]); Mott

insulator, intervalley coherent state and quantum anomalous Hall (QAH) insulator can be stabilized at $\nu = 1$ (Ref. [20, 46, 87]); the model could also support flat bands with uniform momentum distribution of Berry curvatures that stabilize fractional QAH states [88]. The understanding on the complex phase diagram is far from complete. Experimental realization of the Kane-Mele-Hubbard model is therefore of tremendous interests.

AB-stacked hetero-bilayers. Surprisingly, the first experimental realization of Kane-Mele-Hubbard physics in semiconductor moiré materials did not happen in AA-stacked TMD homo-bilayers under near zero vertical electric field, as proposed by theory, but in rather opposite experimental conditions: AB-stacked $MoTe_2/WSe_2$ hetero-bilayers under a large vertical electric field [56]. In particular, evidence of an electric-field-induced continuous topological phase transition from a moiré band insulator to a quantum spin Hall insulator is observed at $\nu = 2$, demonstrating the emergence of topological moiré bands (Fig. 4c). At $\nu = 1$, a robust QAH state that exhibits zero-magnetic-field quantized Hall transport and small longitudinal resistance up to ~ 2 K emerges (Fig. 4e, f); the temperature scale is comparable to that in twisted bilayer graphene [89, 90]. An electric-field-induced topological phase transition from a Mott insulator to a QAH insulator without charge gap closure is also observed (Fig. 4d). Such transition is in contrast to the better-known continuous topological phase transitions that involve charge gap closure at the critical point [91] (e.g. that at $\nu = 2$). The absence of a charge gap closure is likely connected to the change in symmetry between the Mott and the QAH insulator [92]. Recent mean-field calculations suggest that the transition is first-order [46, 87]; more in-depth studies are required. The experimental Kane-Mele-Hubbard phase diagram mapped to date is summarized in Fig. 3b. Other exotic electronic states of matter are awaited for discovery by future experiments.

Two different theoretical pictures have been proposed to explain the emergence of topological bands in AB-stacked TMD hetero-bilayers [44, 93]. A tight-binding construction has also been reported [94]. In one theory, the periodic strain in the moiré lattice from atomic lattice relaxations within the monolayer TMDs produces a periodic pseudomagnetic field responsible for the emergence of topological bands with finite valley-resolved Chern numbers [93]. The application of a vertical electric field that tunes the interlayer band alignment does not change this pseudomagnetic field contribution to the moiré potential but changes the periodic interlayer hopping contribution. The interplay of the two contributions gives rise to topological transitions in the single-particle bands. In the other theory based on large-scale DFT calculations, the electronic envelope wave function for the first and second moiré valence band in $MoTe_2/WSe_2$ is from the $MoTe_2$ and the WSe_2 layer, respectively [44]. The two wave functions are centered at the MM and XX sites of the AB-stacked structure, forming a honeycomb lattice. A vertical electric field that tunes the interlayer band alignment causes band inversion. Interlayer tunneling is allowed because of lattice corrugation in the moiré structure; a gap is reopened after band inversion and topological bands emerge. The situation bears similarity to the AA-stacked case [20, 46]; the Kane-Mele-Hubbard model captures the low-energy physics.

Moiré excitons

In addition to fermionic flat bands, bosonic flat bands can also be realized in TMD moiré materials. Because electrons in the conduction and valence bands in general experience different moiré potentials (in both depth and phase), a spatially periodic band gap modulation arises (Fig. 5a). In the limit that the moiré period is large compared to the exciton Bohr radius, the periodic band gap modulation dominates the contribution to the moiré potential for excitons (bound electron-hole pairs), and gives excitonic moiré bands [95, 96] (Fig. 5a). The emergence of excitonic moiré bands modifies the optical selection rules [95-97]. In particular, umklapp scattering off the superlattice provides additional momentum to activate the otherwise momentum-dark excitons in monolayer TMDs [95-98]. Since the optical wavelength remains much larger than the moiré period, only zone-center excitons in the moiré Brillouin zone are optically active (Fig. 5a). Therefore, compared to a single dominant excitonic resonance in the optical absorption spectrum of monolayer TMDs [27, 51], multiple moiré exciton resonances are expected in TMD moiré materials [95, 97]. Although umklapp scattering induces additional excitonic resonances, the valley-dependent optical selection rule remains unchanged in TMD moiré systems because the moiré period is much larger than the atomic length scale so that the valley pseudospin remains a good quantum number [95-97]. In the following, we review recent progress on the experimental studies of moiré excitons, with a particular focus on equilibrium exciton fluid in a moiré lattice. We refer readers who are interested in optically excited excitons to a recent review article [99].

Optically excited moiré excitons. Experimental studies based on optical absorption and radiative recombination of excitons in TMD moiré materials has demonstrated the emergence of excitonic moiré bands [34-37]. In particular, intralayer moiré excitons, which involve transitions between excitonic moiré bands within a single TMD layer [34, 35] (Fig. 5b); interlayer moiré excitons [36, 37], which involve transitions between states from two different TMD layers; layer-hybridized moiré excitons [35, 100], which involve transitions between layer-hybridized electronic states; moiré exciton-polaritons [101], strongly coupled moiré excitons and photons; and charged moiré excitons [102-105], which are bound states of moiré excitons with electron/holes, have all been reported by recent experiments on various TMD combinations (e.g. WSe_2/WS_2, $MoSe_2/WS_2$ and $MoSe_2/WSe_2$ etc.). Control of the layer-hybridized moiré excitons by the quantum confined Stark effect has also been demonstrated [31, 100]. Moreover, two different types of behaviors have been reported in photoluminescence (PL) studies. In twisted $MoSe_2/WSe_2$, interlayer excitons trapped by disordered moiré potentials, giving rise to a series of sharp PL peaks, have been observed at low optical pumping intensity [37, 102-105]. At high pumping intensity, the disordered moiré sites with a random distribution of trapping depths become increasingly populated with excitons, leading to a smooth PL peak that corresponds to a continuous distribution of the defect emissions [104]. This behavior is in contrast to that in angle-aligned WSe_2/WS_2, in which only a smooth interlayer exciton PL peak is observed down to the lowest optical pumping intensity [32]. The origin of the different behaviors in the two materials deserves further investigation.

Equilibrium moiré excitons. In addition to non-equilibrium moiré excitons created by optical pumping, equilibrium moiré excitons with density determined by the electrostatics

in a capacitor device (rather than by pumping) have also been reported by recent experiments [106, 107]. Such equilibrium exciton fluid on a moiré lattice has the potentials to realize the many exotic bosonic phases of matter (e.g. bosonic Mott insulators, Wigner crystals, superfluids and supersolids etc.) predicted in the Bose-Hubbard model [108, 109] (Hubbard model for bosons) and the SU(4) Hubbard model [50] (two-orbital Fermi-Hubbard model). Equilibrium moiré excitons can be realized in either a Coulomb-coupled double moiré system [50] or a Coulomb-coupled moiré-monolayer system [106, 107]. The spatially separated electrons and holes in these bilayer structures form interlayer excitons in a lattice (Fig. 5c). In order to quench the single-particle tunneling between the constituent layers, they are separated by a thin tunnel barrier (typically hBN); the Coulomb coupling dominates over the single-particle tunneling. In the limit that the barrier thickness is small compared to the moiré period, the interlayer Coulomb correlation becomes as strong as the intralayer counterpart. The Coulomb-coupled bilayer can be contacted by a single common electrode or by separate electrodes to the electron and hole layer; the electrodes act as an electrical reservoir for excitons [110-112]. This reservoir allows the top and bottom gates, which can separately control the total doping density (or total filling factor) and the vertical electric field in the bilayer structure, to continuously tune the exciton density and chemical potential. An equilibrium exciton fluid with density determined by electrostatics is realized.

There are two ways to create an equilibrium exciton fluid in the Coulomb-coupled bilayer. The first is to create an electron-hole double layer by electron-doping one layer and hole-doping the other layer [111]. Whereas this has been realized in Coulomb-coupled TMD double layers without a moiré lattice, its realization in a moiré lattice remains to be demonstrated. The second method relies on a particle-hole transformation [106, 107, 113] (Fig. 5c). Consider a Coulomb-coupled moiré-monolayer system with the moiré layer doped at filling factor $\nu = 1$ (one electron/hole per moiré site) and the monolayer charge neutral; the entire system is at total filling factor 1. This configuration can be readily realized with the two gates and the electrical reservoir. Under a vertical electric field, some charges ($\delta\nu$) can be transferred from the moiré layer to the monolayer. The moiré lattice allows us to view the system as filled with $1 - \delta\nu$ particles in the moiré layer and $\delta\nu$ particles in the monolayer or as $\delta\nu$ holes (or empty moiré sites) in the moiré layer and $\delta\nu$ particles in the monolayer. The particles and holes in the latter particle-hole transformed configuration are Coulomb bound in order to minimize the interlayer Coulomb repulsions in the system; an equilibrium exciton fluid in a lattice is formed. This approach of creating an equilibrium exciton fluid in a moiré lattice has recently been demonstrated by two independent experiments using Coulomb-coupled WSe_2/WS_2 moiré layer and WSe_2 monolayer [106, 107]. Both optical and capacitance measurements have shown the emergence of a charge-incompressible state at total filling factor 1 when the system is filled with an exciton fluid; the state is consistent with an excitonic insulating state (Fig. 5d). The dipolar excitons are expected to be strongly correlated in the sense that the dipole-dipole repulsion energy is much larger than the exciton kinetic energy. The results pave the path to explore the Bose-Hubbard [108, 109] and the SU(4) Hubbard [50] phase diagrams in moiré materials.

Outlook

We believe it is only the beginning of semiconductor moiré materials. There are plenty of opportunities and challenges for both TMD-based and beyond-TMD semiconductor moiré systems. Within the TMD moiré family, much of the Hubbard and Kane-Mele-Hubbard phase diagram remains unexplored. Outstanding problems include, for example, the nature of the bandwidth-tuned Mott and Wigner transitions; spin liquid physics near the Mott transition; the existence of superconductivity near the Mott insulator in a triangular lattice; exotic excitonic phases of matter (e.g. exciton Mott insulators, exciton solids and exciton supersolids); fractional QAH physics; and many more. The ability to continuously tune the filling factor as well as terms in the many-body Hamiltonian will very much likely allow the exploration of these problems in new ways. In addition to Hubbard physics, recent theoretical studies have also proposed the realization of Kondo lattice physics in moiré systems with exchange-coupled itinerant band and local moment flat band [114, 115], and layer pseudospin liquid physics in Coulomb-coupled moiré double layers [50, 116]. These interesting structures remain to be explored.

Looking beyond TMD semiconductors, there is a large family of 2D semiconductors with different properties and crystal symmetries. These include, for instance, black phosphorous with a buckled in-plane anisotropic structure [117], III-VI semiconductors with band edges near the Γ-point of the Brillouin zone [118], and a large family of layered magnetic semiconductors with different crystal and magnetic structures [119, 120]. This large set of building blocks will allow us to explore moiré superlattices with symmetries different from the triangular lattice, for example, distorted triangular lattice, square lattice and quasi-1D lattice. The family of magnetic semiconductors is also an attractive platform to explore moiré magnetism. Indeed, recent theoretical studies that made use of the stacking-structure-dependent interlayer exchange interaction in layered magnetic materials have predicted a suite of exotic magnetic ground states in twisted magnetic materials [121-123], such as non-collinear magnetic ground state, skyrmion lattice and multi-flavor magnetic state. These states can support novel moiré magnon bands and complex magnon networks [124]. Recent experiments have demonstrated the coexistence of ferromagnetic and antiferromagnetic states in small-angle twisted bilayer CrI_3, providing evidence of a non-collinear magnetic state [125-127]. These results demonstrate the great potentials of magnetic moiré semiconductors in engineering magnetism in the nanoscale. We anticipate exciting developments in this direction in the near future.

Outstanding promises are accompanied by outstanding challenges. One of the most significant and longstanding challenges in the field of 2D semiconductor materials is the formation of good electrical contacts for transport and thermodynamics studies. Substantial progress has been made in recent years but further improvements are required. Another important challenge is material quality. In particular, effects of disorder broadening of the electronic energy levels are much more significant in moiré materials with flat bands. Coherent band physics becomes relevant only when such broadening is small compared to the moiré bandwidth. Improvements in both the semiconductor quality and the homogeneity of the moiré superlattice structure are required. Over the years, the material quality of bulk and monolayer TMD crystals has been dramatically improved [128]; improvements in other 2D semiconductor materials will substantially expand the list of

interesting semiconductor moiré materials. In terms of improving the homogeneity of the moiré superlattice structure, we believe thermal annealing induced structural relaxation is a promising route in hetero-bilayers with significant lattice mismatch because the lowest energy structure is the angle-aligned structure. Systematic exploration is required.

Figures

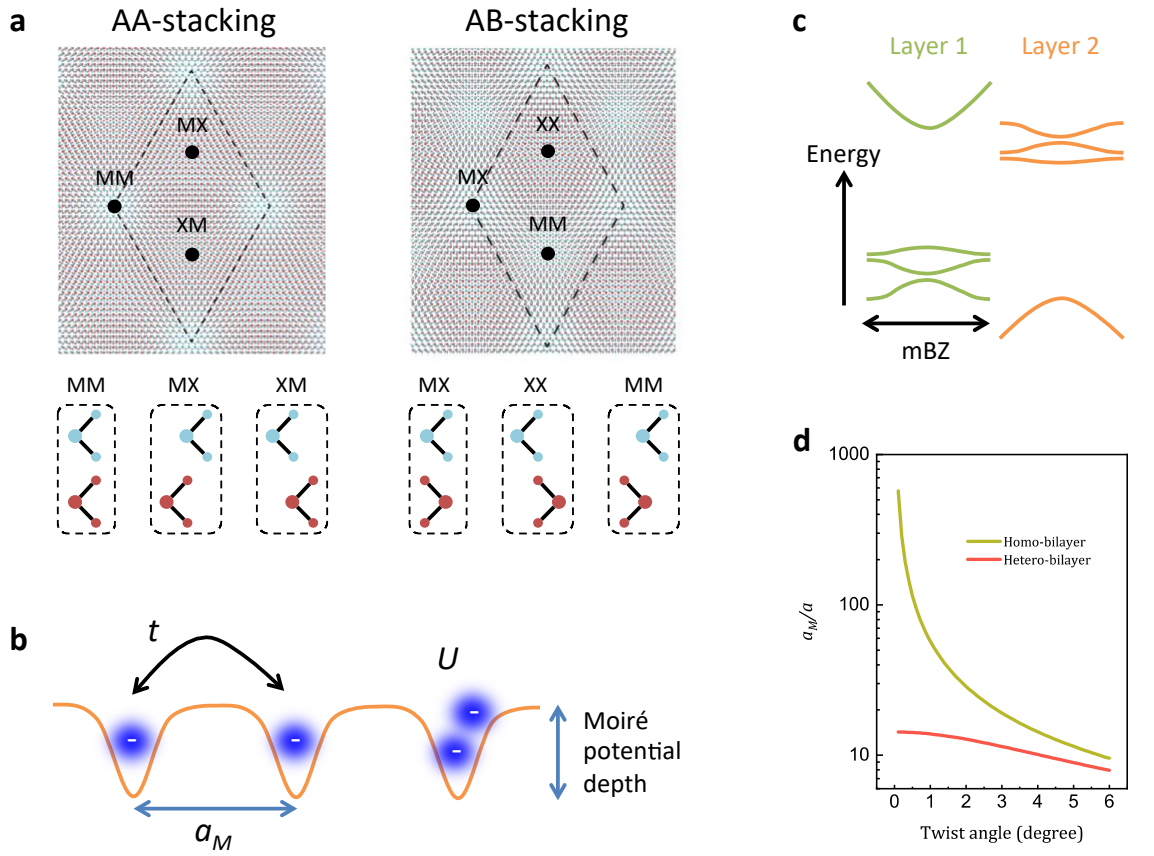

Figure 1 | TMD semiconductor moiré materials. a, Moiré lattice structure for AA- and AB-stacked TMD semiconductor moiré materials (top). The high-symmetry sites for each case are labeled; their cross-section views are illustrated (bottom). The large and small dots label the transition metal atom (M = Mo and W) and the chalcogen atom (X = S, Se and Te), respectively. **b,** Schematic illustration of an array of moiré atoms that can trap electrons, which can tunnel between neighboring sites with amplitude t and experience on-site Coulomb repulsion U. **c,** Schematic layer-resolved moiré band structure for semiconductor moiré materials with type-II band alignment. mBZ stands for mini-Brillouin zone. **d,** Twist angle dependence of the normalized moiré period a_M/a for both homo- and hetero-bilayers (in the small angle limit, $\delta = 7\%$). a_M/a is much more sensitive to twist angle variations in homo-bilayers.

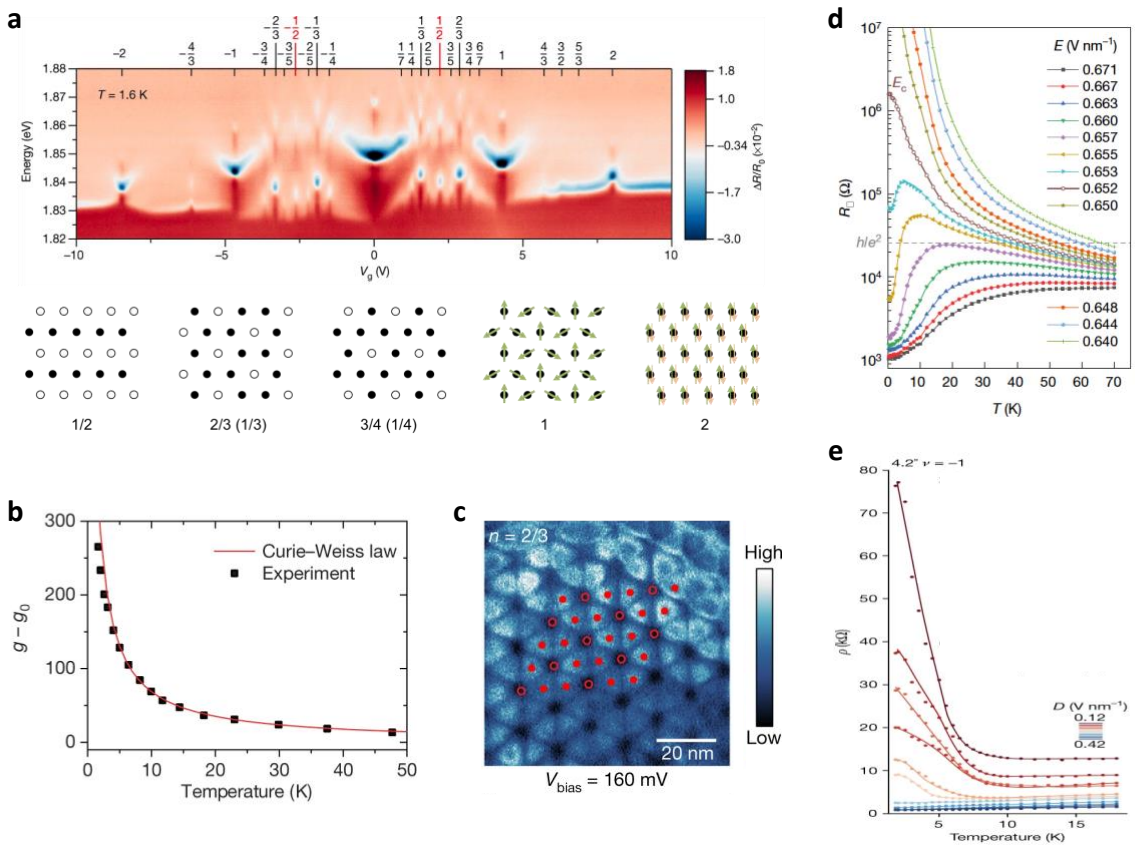

Figure 2 | Hubbard model physics. a, (Top) Gate voltage dependence of the reflection contrast spectrum of a Rydberg sensor (monolayer WSe_2) proximal to a WSe_2/WS_2 moiré superlattice. An abundance of insulating states is seen by blueshifts of the 2s exciton resonance and enhancements in the spectral weight. The top axis shows the filling factor for the insulating states. (Bottom) Ground state charge-order configuration at varying filling factors. Filled and unfilled circles denote occupied and empty sites for state ν, respectively. The notation of the occupied and empty sites is switched for the state $1-\nu$. The ground state spin configuration (arrows) is also shown for the Mott state and the band insulating state. **b,** Temperature dependence of the moiré exciton g-factor (proportional to the spin susceptibility) for the Mott insulating state in WSe_2/WS_2 moiré superlattice. The solid line is a Curie-Weiss fit to the data points. **c,** STM image of the charge-order configuration (illustrated by the filled and unfilled circles) for the $\nu = 2/3$ generalized Wigner crystal state in WSe_2/WS_2 moiré superlattice. **d, e,** Temperature dependent resistivity at varying perpendicular electric fields applied to $MoTe_2/WSe_2$ moiré (**d**) and twisted-WSe_2 moiré (**e**). A sharp metal-insulator transition is observed at fixed half-band-filling.

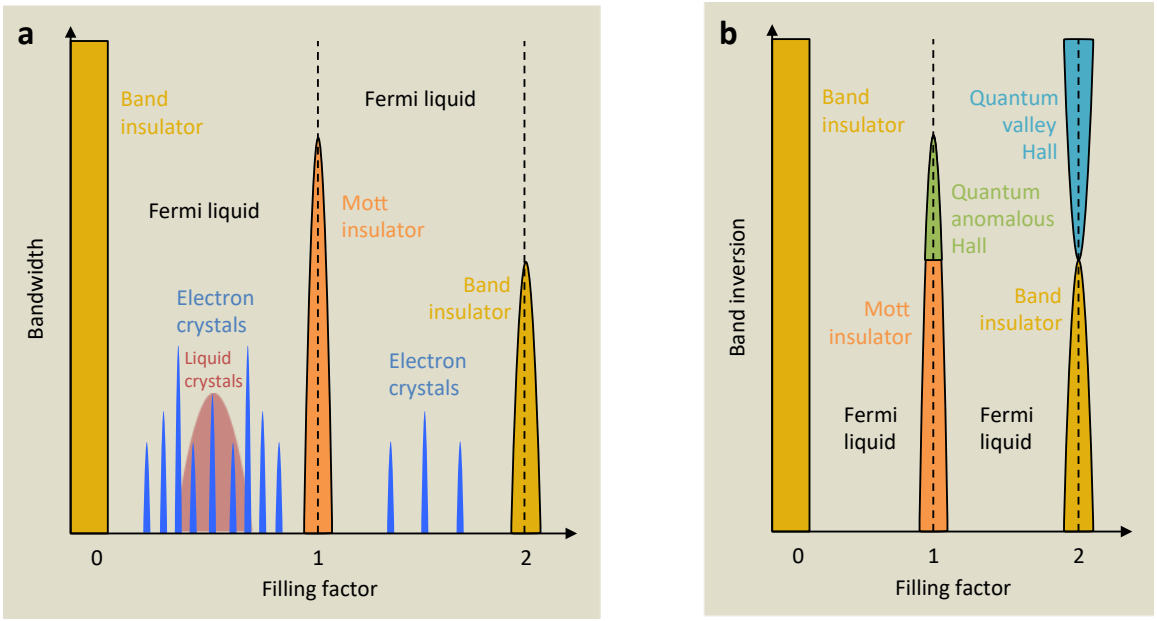

Figure 3 | Partial moiré Hubbard and Kane-Mele-Hubbard phase diagrams. a, Schematic triangular lattice Hubbard phase diagram (in the bandwidth-filling factor plane) revealed by experiments on various TMD semiconductor moiré materials to date. Note that the Wigner transitions at fractional fillings have not been examined in details so far. **b,** Schematic Kane-Mele-Hubbard phase diagram (in the band inversion-filling factor plane) revealed by experiments on AB-stacked $MoTe_2/WSe_2$ moiré to date. The different insulating states are labeled by different colors.

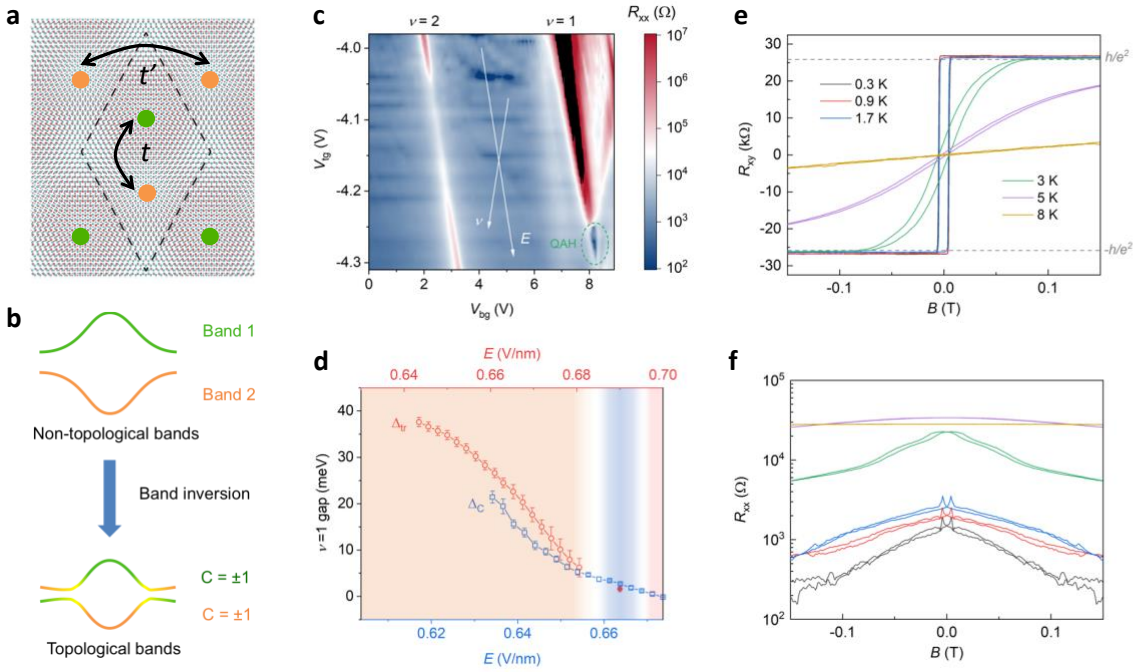

Figure 4 | Kane-Mele-Hubbard physics. a, Illustration of the Kane-Mele model in a honeycomb lattice on a semiconductor moiré system. The orange and green circles denote the two sublattice sites in a honeycomb; the two sites are in general at different electrostatic potentials tunable by a perpendicular electric field. t and t' denote the nearest and next-nearest neighbor hopping, respectively. **b,** Schematic illustration of intertwining two moiré flat bands by band inversion and interlayer hybridization. The bands become topological with finite valley-resolved Chern numbers after band inversion. **c,** Dependence of the 300 mK longitudinal resistance of AB-stacked $MoTe_2/WSe_2$ moiré on the top and bottom gate voltages. The electric field and filling factor directions are labeled by the arrows. The QAH region with vanishing resistance is circled by the green dashed line. **d,** Electric field dependence of the charge gap at half-band-filling from the Mott insulating region (orange shaded) to the QAH region (blue shaded) and the metallic region (pink shaded). No charge gap closure is observed at the Mott-QAH boundary. The red and blue data points are obtained by thermal activation fits to the resistance data and by direct compressibility measurements, respectively. **e, f,** Magnetic field dependence of the Hall (**e**) and longitudinal (**f**) resistances at varying temperatures for the QAH state. Nearly quantized Hall resistance and vanishing longitudinal resistance are observed at low temperatures.

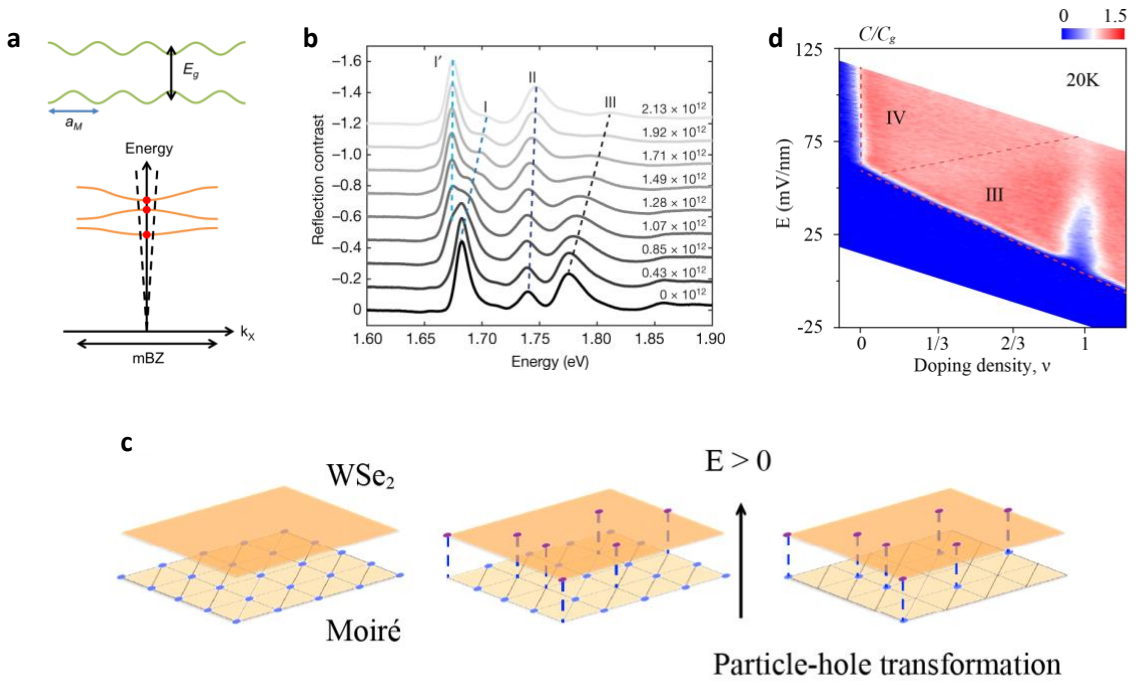

Figure 5 | Excitons in a moiré lattice. a, Schematic illustration of band gap modulation in moiré length scales (top) and formation of exciton flat bands in the mini-Brillouin zone (bottom). The light cone is labeled by the dashed lines and the momentum-allowed excitonic transitions are denoted by the red dots. **b,** Reflection contrast spectrum of WSe_2/WS_2 moiré at varying electron doping densities. The spectra are vertically shifted for clarity. The three exciton replicas (I, II and III) are the intralayer moiré exciton resonances in the WSe_2 layer. **c,** Mott insulating state at half-band-filling when all electrons reside in the moiré layer (left). The transferred electrons to the TMD monolayer under an electric field are tightly bound to the empty moiré sites to minimize the total Coulomb repulsion energy (middle). Under a particle-hole transformation, the empty sites in the moiré layer become holes; a dipolar exciton fluid emerges in the moiré lattice. **d,** Penetration capacitance normalized by the geometrical capacitance as a function of perpendicular electric field and the total filling factor in the Coulomb-coupled WSe_2/WS_2 moiré-WSe_2 monolayer system. Both the moiré layer and the monolayer are hole-doped in region III. An incompressible state is observed at total filling factor 1, corresponding to an excitonic insulating state.

Table

	Twisted bilayer graphene	**TMD semiconductor moiré mateirals**
Sensitivity on twist angle	Magic angle(s) for flat bands Sensitive to twist angle variations	No magic angle in general Homo(hetero)-bilayer: sensitive (insensitive) to twist angle variations
Local tight-binding description of low-energy physics	Generally not possible because of Wannier obstruction	Good approximation
Electronic degrees of freedom	Spin *and* valley degenerate	Spin-valley locked Spin *or* valley degenerate
Typical energy scales	W ~ 1-100 meV U ~ 20-40 meV	W ~ 1-100 meV U ~ 100-200 meV

Table I | Comparison between twisted bilayer graphene and TMD semiconductor moiré materials.

References

1. Cao, Y., Fatemi, V., Demir, A., Fang, S., Tomarken, S.L., Luo, J.Y., Sanchez-Yamagishi, J.D., Watanabe, K., Taniguchi, T., Kaxiras, E., Ashoori, R.C. & Jarillo-Herrero, P. Correlated insulator behaviour at half-filling in magic-angle graphene superlattices. *Nature* **556**, 80-84 (2018).
2. Cao, Y., Fatemi, V., Fang, S., Watanabe, K., Taniguchi, T., Kaxiras, E. & Jarillo-Herrero, P. Unconventional superconductivity in magic-angle graphene superlattices. *Nature* **556**, 43-50 (2018).
3. Chen, G., Jiang, L., Wu, S., Lyu, B., Li, H., Chittari, B.L., Watanabe, K., Taniguchi, T., Shi, Z., Jung, J., Zhang, Y. & Wang, F. Evidence of a gate-tunable Mott insulator in a trilayer graphene moiré superlattice. *Nature Physics* **15**, 237-241 (2019).
4. Bistritzer, R. & MacDonald, A.H. Moiré bands in twisted double-layer graphene. *Proceedings of the National Academy of Sciences* **108**, 12233 (2011).
5. Li, T., Jiang, S., Li, L., Zhang, Y., Kang, K., Zhu, J., Watanabe, K., Taniguchi, T., Chowdhury, D., Fu, L., Shan, J. & Mak, K.F. Continuous Mott transition in semiconductor moiré superlattices. *Nature* **597**, 350-354 (2021).
6. Ghiotto, A., Shih, E.-M., Pereira, G.S.S.G., Rhodes, D.A., Kim, B., Zang, J., Millis, A.J., Watanabe, K., Taniguchi, T., Hone, J.C., Wang, L., Dean, C.R. & Pasupathy, A.N. Quantum criticality in twisted transition metal dichalcogenides. *Nature* **597**, 345-349 (2021).
7. Yankowitz, M., Chen, S., Polshyn, H., Zhang, Y., Watanabe, K., Taniguchi, T., Graf, D., Young Andrea, F. & Dean Cory, R. Tuning superconductivity in twisted bilayer graphene. *Science* **363**, 1059-1064 (2019).
8. Andrei, E.Y., Efetov, D.K., Jarillo-Herrero, P., MacDonald, A.H., Mak, K.F., Senthil, T., Tutuc, E., Yazdani, A. & Young, A.F. The marvels of moiré materials. *Nature Reviews Materials* **6**, 201-206 (2021).
9. Andrei, E.Y. & MacDonald, A.H. Graphene bilayers with a twist. *Nature Materials* **19**, 1265-1275 (2020).
10. Balents, L., Dean, C.R., Efetov, D.K. & Young, A.F. Superconductivity and strong correlations in moiré flat bands. *Nature Physics* **16**, 725-733 (2020).
11. Zhang, Y., Yuan, N.F.Q. & Fu, L. Moir\'e quantum chemistry: Charge transfer in transition metal dichalcogenide superlattices. *Physical Review B* **102**, 201115 (2020).
12. Novoselov, K.S., Geim, A.K., Morozov, S.V., Jiang, D., Zhang, Y., Dubonos, S.V., Grigorieva, I.V. & Firsov, A.A. Electric Field Effect in Atomically Thin Carbon Films. *Science* **306**, 666-669 (2004).
13. Novoselov, K.S., Geim, A.K., Morozov, S.V., Jiang, D., Katsnelson, M.I., Grigorieva, I.V., Dubonos, S.V. & Firsov, A.A. Two-dimensional gas of massless Dirac fermions in graphene. *Nature* **438**, 197-200 (2005).
14. Zhang, Y., Tan, Y.-W., Stormer, H.L. & Kim, P. Experimental observation of the quantum Hall effect and Berry's phase in graphene. *Nature* **438**, 201-204 (2005).
15. Li, G., Luican, A., Lopes dos Santos, J.M.B., Castro Neto, A.H., Reina, A., Kong, J. & Andrei, E.Y. Observation of Van Hove singularities in twisted graphene layers. *Nature Physics* **6**, 109-113 (2010).

16. Suárez Morell, E., Correa, J.D., Vargas, P., Pacheco, M. & Barticevic, Z. Flat bands in slightly twisted bilayer graphene: Tight-binding calculations. *Physical Review B* **82**, 121407 (2010).
17. Mele, E.J. Commensuration and interlayer coherence in twisted bilayer graphene. *Physical Review B* **81**, 161405 (2010).
18. Lu, X., Stepanov, P., Yang, W., Xie, M., Aamir, M.A., Das, I., Urgell, C., Watanabe, K., Taniguchi, T., Zhang, G., Bachtold, A., MacDonald, A.H. & Efetov, D.K. Superconductors, orbital magnets and correlated states in magic-angle bilayer graphene. *Nature* **574**, 653-657 (2019).
19. Wu, F., Lovorn, T., Tutuc, E. & MacDonald, A.H. Hubbard Model Physics in Transition Metal Dichalcogenide Moir\'e Bands. *Physical Review Letters* **121**, 026402 (2018).
20. Wu, F., Lovorn, T., Tutuc, E., Martin, I. & MacDonald, A.H. Topological Insulators in Twisted Transition Metal Dichalcogenide Homobilayers. *Physical Review Letters* **122**, 086402 (2019).
21. Xian, L., Kennes, D.M., Tancogne-Dejean, N., Altarelli, M. & Rubio, A. Multiflat Bands and Strong Correlations in Twisted Bilayer Boron Nitride: Doping-Induced Correlated Insulator and Superconductor. *Nano Letters* **19**, 4934-4940 (2019).
22. Zou, L., Po, H.C., Vishwanath, A. & Senthil, T. Band structure of twisted bilayer graphene: Emergent symmetries, commensurate approximants, and Wannier obstructions. *Physical Review B* **98**, 085435 (2018).
23. Mak, K.F., Lee, C., Hone, J., Shan, J. & Heinz, T.F. Atomically thin MoS 2: a new direct-gap semiconductor. *Physical review letters* **105**, 136805 (2010).
24. Splendiani, A., Sun, L., Zhang, Y., Li, T., Kim, J., Chim, C.-Y., Galli, G. & Wang, F. Emerging Photoluminescence in Monolayer MoS2. *Nano Letters* **10**, 1271-1275 (2010).
25. Gustafsson, M.V., Yankowitz, M., Forsythe, C., Rhodes, D., Watanabe, K., Taniguchi, T., Hone, J., Zhu, X. & Dean, C.R. Ambipolar Landau levels and strong band-selective carrier interactions in monolayer WSe2. *Nature Materials* **17**, 411-415 (2018).
26. Xiao, D., Liu, G.-B., Feng, W., Xu, X. & Yao, W. Coupled Spin and Valley Physics in Monolayers of ${\mathrm{MoS}}_{2}$ and Other Group-VI Dichalcogenides. *Physical Review Letters* **108**, 196802 (2012).
27. Mak, K.F., Xiao, D. & Shan, J. Light–valley interactions in 2D semiconductors. *Nature Photonics* **12**, 451-460 (2018).
28. Xu, X., Yao, W., Xiao, D. & Heinz, T.F. Spin and pseudospins in layered transition metal dichalcogenides. *Nature Physics* **10**, 343-350 (2014).
29. Wang, L., Shih, E.-M., Ghiotto, A., Xian, L., Rhodes, D.A., Tan, C., Claassen, M., Kennes, D.M., Bai, Y., Kim, B., Watanabe, K., Taniguchi, T., Zhu, X., Hone, J., Rubio, A., Pasupathy, A.N. & Dean, C.R. Correlated electronic phases in twisted bilayer transition metal dichalcogenides. *Nature Materials* **19**, 861-866 (2020).
30. Zhang, Z., Wang, Y., Watanabe, K., Taniguchi, T., Ueno, K., Tutuc, E. & LeRoy, B.J. Flat bands in twisted bilayer transition metal dichalcogenides. *Nature Physics* **16**, 1093-1096 (2020).

31. Shimazaki, Y., Schwartz, I., Watanabe, K., Taniguchi, T., Kroner, M. & Imamoğlu, A. Strongly correlated electrons and hybrid excitons in a moiré heterostructure. *Nature* **580**, 472-477 (2020).
32. Tang, Y., Li, L., Li, T., Xu, Y., Liu, S., Barmak, K., Watanabe, K., Taniguchi, T., MacDonald, A.H. & Shan, J. Simulation of Hubbard model physics in WSe 2/WS 2 moiré superlattices. *Nature* **579**, 353-358 (2020).
33. Regan, E.C., Wang, D., Jin, C., Bakti Utama, M.I., Gao, B., Wei, X., Zhao, S., Zhao, W., Zhang, Z., Yumigeta, K., Blei, M., Carlström, J.D., Watanabe, K., Taniguchi, T., Tongay, S., Crommie, M., Zettl, A. & Wang, F. Mott and generalized Wigner crystal states in WSe2/WS2 moiré superlattices. *Nature* **579**, 359-363 (2020).
34. Jin, C., Regan, E.C., Yan, A., Iqbal Bakti Utama, M., Wang, D., Zhao, S., Qin, Y., Yang, S., Zheng, Z., Shi, S., Watanabe, K., Taniguchi, T., Tongay, S., Zettl, A. & Wang, F. Observation of moiré excitons in WSe2/WS2 heterostructure superlattices. *Nature* **567**, 76-80 (2019).
35. Alexeev, E.M., Ruiz-Tijerina, D.A., Danovich, M., Hamer, M.J., Terry, D.J., Nayak, P.K., Ahn, S., Pak, S., Lee, J., Sohn, J.I., Molas, M.R., Koperski, M., Watanabe, K., Taniguchi, T., Novoselov, K.S., Gorbachev, R.V., Shin, H.S., Fal'ko, V.I. & Tartakovskii, A.I. Resonantly hybridized excitons in moiré superlattices in van der Waals heterostructures. *Nature* **567**, 81-86 (2019).
36. Tran, K., Moody, G., Wu, F., Lu, X., Choi, J., Kim, K., Rai, A., Sanchez, D.A., Quan, J., Singh, A., Embley, J., Zepeda, A., Campbell, M., Autry, T., Taniguchi, T., Watanabe, K., Lu, N., Banerjee, S.K., Silverman, K.L., Kim, S., Tutuc, E., Yang, L., MacDonald, A.H. & Li, X. Evidence for moiré excitons in van der Waals heterostructures. *Nature* **567**, 71-75 (2019).
37. Seyler, K.L., Rivera, P., Yu, H., Wilson, N.P., Ray, E.L., Mandrus, D.G., Yan, J., Yao, W. & Xu, X. Signatures of moiré-trapped valley excitons in MoSe2/WSe2 heterobilayers. *Nature* **567**, 66-70 (2019).
38. Kim, K., Yankowitz, M., Fallahazad, B., Kang, S., Movva, H.C.P., Huang, S., Larentis, S., Corbet, C.M., Taniguchi, T., Watanabe, K., Banerjee, S.K., LeRoy, B.J. & Tutuc, E. van der Waals Heterostructures with High Accuracy Rotational Alignment. *Nano Letters* **16**, 1989-1995 (2016).
39. Cao, Y., Luo, J.Y., Fatemi, V., Fang, S., Sanchez-Yamagishi, J.D., Watanabe, K., Taniguchi, T., Kaxiras, E. & Jarillo-Herrero, P. Superlattice-Induced Insulating States and Valley-Protected Orbits in Twisted Bilayer Graphene. *Physical Review Letters* **117**, 116804 (2016).
40. Chung, T.-F., Xu, Y. & Chen, Y.P. Transport measurements in twisted bilayer graphene: Electron-phonon coupling and Landau level crossing. *Physical Review B* **98**, 035425 (2018).
41. Rosenberger, M.R., Chuang, H.-J., Phillips, M., Oleshko, V.P., McCreary, K.M., Sivaram, S.V., Hellberg, C.S. & Jonker, B.T. Twist Angle-Dependent Atomic Reconstruction and Moiré Patterns in Transition Metal Dichalcogenide Heterostructures. *ACS Nano* **14**, 4550-4558 (2020).
42. Li, H., Li, S., Naik, M.H., Xie, J., Li, X., Wang, J., Regan, E., Wang, D., Zhao, W., Zhao, S., Kahn, S., Yumigeta, K., Blei, M., Taniguchi, T., Watanabe, K., Tongay, S., Zettl, A., Louie, S.G., Wang, F. & Crommie, M.F. Imaging moiré flat

bands in three-dimensional reconstructed WSe2/WS2 superlattices. *Nature Materials* **20**, 945-950 (2021).
43. Bai, Y., Zhou, L., Wang, J., Wu, W., McGilly, L.J., Halbertal, D., Lo, C.F.B., Liu, F., Ardelean, J., Rivera, P., Finney, N.R., Yang, X.-C., Basov, D.N., Yao, W., Xu, X., Hone, J., Pasupathy, A.N. & Zhu, X.Y. Excitons in strain-induced one-dimensional moiré potentials at transition metal dichalcogenide heterojunctions. *Nature Materials* **19**, 1068-1073 (2020).
44. Zhang, Y., Devakul, T. & Fu, L. Spin-textured Chern bands in AB-stacked transition metal dichalcogenide bilayers. *Proceedings of the National Academy of Sciences* **118**, e2112673118 (2021).
45. Pan, H., Wu, F. & Das Sarma, S. Band topology, Hubbard model, Heisenberg model, and Dzyaloshinskii-Moriya interaction in twisted bilayer ${\mathrm{WSe}}_{2}$. *Physical Review Research* **2**, 033087 (2020).
46. Devakul, T., Crépel, V., Zhang, Y. & Fu, L. Magic in twisted transition metal dichalcogenide bilayers. *Nature Communications* **12**, 6730 (2021).
47. Pan, H., Wu, F. & Das Sarma, S. Quantum phase diagram of a Moir\'e-Hubbard model. *Physical Review B* **102**, 201104 (2020).
48. Slagle, K. & Fu, L. Charge transfer excitations, pair density waves, and superconductivity in moir\'e materials. *Physical Review B* **102**, 235423 (2020).
49. Kennes, D.M., Claassen, M., Xian, L., Georges, A., Millis, A.J., Hone, J., Dean, C.R., Basov, D.N., Pasupathy, A.N. & Rubio, A. Moiré heterostructures as a condensed-matter quantum simulator. *Nature Physics* **17**, 155-163 (2021).
50. Zhang, Y.-H., Sheng, D.N. & Vishwanath, A. SU(4) Chiral Spin Liquid, Exciton Supersolid, and Electric Detection in Moir\'e Bilayers. *Physical Review Letters* **127**, 247701 (2021).
51. Mak, K.F. & Shan, J. Photonics and optoelectronics of 2D semiconductor transition metal dichalcogenides. *Nature Photonics* **10**, 216-226 (2016).
52. Xu, Y., Liu, S., Rhodes, D.A., Watanabe, K., Taniguchi, T., Hone, J., Elser, V., Mak, K.F. & Shan, J. Correlated insulating states at fractional fillings of moiré superlattices. *Nature* **587**, 214-218 (2020).
53. Li, T., Zhu, J., Tang, Y., Watanabe, K., Taniguchi, T., Elser, V., Shan, J. & Mak, K.F. Charge-order-enhanced capacitance in semiconductor moiré superlattices. *Nature Nanotechnology* **16**, 1068-1072 (2021).
54. Stepanov, P., Das, I., Lu, X., Fahimniya, A., Watanabe, K., Taniguchi, T., Koppens, F.H.L., Lischner, J., Levitov, L. & Efetov, D.K. Untying the insulating and superconducting orders in magic-angle graphene. *Nature* **583**, 375-378 (2020).
55. Saito, Y., Ge, J., Watanabe, K., Taniguchi, T. & Young, A.F. Independent superconductors and correlated insulators in twisted bilayer graphene. *Nature Physics* **16**, 926-930 (2020).
56. Li, T., Jiang, S., Shen, B., Zhang, Y., Li, L., Tao, Z., Devakul, T., Watanabe, K., Taniguchi, T. & Fu, L. Quantum anomalous Hall effect from intertwined moiré bands. *Nature* **600**, 641-646 (2021).
57. Mott, N.F. Metal-Insulator Transition. *Reviews of Modern Physics* **40**, 677-683 (1968).

58. Imada, M., Fujimori, A. & Tokura, Y. Metal-insulator transitions. *Reviews of Modern Physics* **70**, 1039-1263 (1998).
59. Senthil, T. Theory of a continuous Mott transition in two dimensions. *Physical Review B* **78**, 045109 (2008).
60. Mishmash, R.V., González, I., Melko, R.G., Motrunich, O.I. & Fisher, M.P.A. Continuous Mott transition between a metal and a quantum spin liquid. *Physical Review B* **91**, 235140 (2015).
61. Lee, P.A. Moiré bands in transitional metal dichalcogenides: continuous Mott transition, quantum anomalous Hall and more. *Journal Club for Condensed Matter Physics,* https://doi.org/10.36471/JCCM_September_2021_03 (2021).
62. Balents, L. Spin liquids in frustrated magnets. *Nature* **464**, 199-208 (2010).
63. Szasz, A., Motruk, J., Zaletel, M.P. & Moore, J.E. Chiral Spin Liquid Phase of the Triangular Lattice Hubbard Model: A Density Matrix Renormalization Group Study. *Physical Review X* **10**, 021042 (2020).
64. Yiqing Zhou, D. N. Sheng & Kim, E.-A. Quantum Phases of Transition Metal Dichalcogenide Moiré Systems. *arXiv:2105.07008* (2021).
65. Morales-Durán, N., MacDonald, A.H. & Potasz, P. Metal-insulator transition in transition metal dichalcogenide heterobilayer moir\'e superlattices. *Physical Review B* **103**, L241110 (2021).
66. Pan, H. & Das Sarma, S. Interaction-Driven Filling-Induced Metal-Insulator Transitions in 2D Moir\'e Lattices. *Physical Review Letters* **127**, 096802 (2021).
67. Wietek, A., Rossi, R., Šimkovic, F., Klett, M., Hansmann, P., Ferrero, M., Stoudenmire, E.M., Schäfer, T. & Georges, A. Mott Insulating States with Competing Orders in the Triangular Lattice Hubbard Model. *Physical Review X* **11**, 041013 (2021).
68. Jiawei Zang, Jie Wang, Jennifer Cano, Antoine Georges & Millis, A.J. Dynamical mean field theory of moiré bilayer transition metal dichalcogenides: phase diagram, resistivity, and quantum criticality. *arXiv:2112.03080* (2021).
69. Seongjin Ahn & Sarma, S.D. Disorder induced 2D metal-insulator transition in moiré transition metal dichalcogenide multilayers. *arXiv:2108.07271* (2021).
70. Sunghoon Kim, D.C. Private discussion. (2021).
71. Zhang, Y., Liu, T. & Fu, L. Electronic structures, charge transfer, and charge order in twisted transition metal dichalcogenide bilayers. *Physical Review B* **103**, 155142 (2021).
72. Padhi, B., Chitra, R. & Phillips, P.W. Generalized Wigner crystallization in moir\'e materials. *Physical Review B* **103**, 125146 (2021).
73. Huang, X., Wang, T., Miao, S., Wang, C., Li, Z., Lian, Z., Taniguchi, T., Watanabe, K., Okamoto, S., Xiao, D., Shi, S.-F. & Cui, Y.-T. Correlated insulating states at fractional fillings of the WS2/WSe2 moiré lattice. *Nature Physics* **17**, 715-719 (2021).
74. Li, H., Li, S., Regan, E.C., Wang, D., Zhao, W., Kahn, S., Yumigeta, K., Blei, M., Taniguchi, T., Watanabe, K., Tongay, S., Zettl, A., Crommie, M.F. & Wang, F. Imaging two-dimensional generalized Wigner crystals. *Nature* **597**, 650-654 (2021).
75. Liu, E., Taniguchi, T., Watanabe, K., Gabor, N.M., Cui, Y.-T. & Lui, C.H. Excitonic and Valley-Polarization Signatures of Fractional Correlated Electronic

Phases in a ${\mathrm{WSe}}_{2}/{\mathrm{WS}}_{2}$ Moir\'e Superlattice. *Physical Review Letters* **127**, 037402 (2021).
76. Emery, V.J., Kivelson, S.A. & Tranquada, J.M. Stripe phases in high-temperature superconductors. *Proceedings of the National Academy of Sciences* **96**, 8814 (1999).
77. Koulakov, A.A., Fogler, M.M. & Shklovskii, B.I. Charge Density Wave in Two-Dimensional Electron Liquid in Weak Magnetic Field. *Physical Review Letters* **76**, 499-502 (1996).
78. Kivelson, S.A., Fradkin, E. & Emery, V.J. Electronic liquid-crystal phases of a doped Mott insulator. *Nature* **393**, 550-553 (1998).
79. Michael Matty & Kim, E.-A. Melting of generalized Wigner crystals in transition metal dichalcogenide heterobilayer Moiré systems. *arXiv:2112.08624* (2021).
80. Jin, C., Tao, Z., Li, T., Xu, Y., Tang, Y., Zhu, J., Liu, S., Watanabe, K., Taniguchi, T., Hone, J.C., Fu, L., Shan, J. & Mak, K.F. Stripe phases in WSe2/WS2 moiré superlattices. *Nature Materials* **20**, 940-944 (2021).
81. Camjayi, A., Haule, K., Dobrosavljević, V. & Kotliar, G. Coulomb correlations and the Wigner–Mott transition. *Nature Physics* **4**, 932-935 (2008).
82. Seth Musser, T. Senthil & Chowdhury, D. Theory of a Continuous Bandwidth-tuned Wigner-Mott Transition. *arXiv:2111.09894* (2021).
83. Wigner, E. On the Interaction of Electrons in Metals. *Physical Review* **46**, 1002-1011 (1934).
84. Kane, C.L. & Mele, E.J. Quantum Spin Hall Effect in Graphene. *Physical Review Letters* **95**, 226801 (2005).
85. Hohenadler, M. & Assaad, F.F. Correlation effects in two-dimensional topological insulators. *Journal of Physics: Condensed Matter* **25**, 143201 (2013).
86. Witczak-Krempa, W., Chen, G., Kim, Y.B. & Balents, L. Correlated Quantum Phenomena in the Strong Spin-Orbit Regime. *Annual Review of Condensed Matter Physics* **5**, 57-82 (2014).
87. Haining Pan, Ming Xie, Fengcheng Wu & Sarma, S.D. Topological Phases in AB-stacked MoTe2/WSe2: ℤ2 Topological Insulators, Chern Insulators, and Topological Charge Density Waves. *arXiv:2111.01152* (2021).
88. Regnault, N. & Bernevig, B.A. Fractional Chern Insulator. *Physical Review X* **1**, 021014 (2011).
89. Serlin, M., Tschirhart, C.L., Polshyn, H., Zhang, Y., Zhu, J., Watanabe, K., Taniguchi, T., Balents, L. & Young, A.F. Intrinsic quantized anomalous Hall effect in a moiré heterostructure. *Science* **367**, 900-903 (2020).
90. Sharpe Aaron, L., Fox Eli, J., Barnard Arthur, W., Finney, J., Watanabe, K., Taniguchi, T., Kastner, M.A. & Goldhaber-Gordon, D. Emergent ferromagnetism near three-quarters filling in twisted bilayer graphene. *Science* **365**, 605-608 (2019).
91. Hasan, M.Z. & Kane, C.L. Colloquium: Topological insulators. *Reviews of Modern Physics* **82**, 3045-3067 (2010).
92. Ezawa, M., Tanaka, Y. & Nagaosa, N. Topological Phase Transition without Gap Closing. *Scientific Reports* **3**, 2790 (2013).

93. Xie, Y.-M., Zhang, C.-P., Hu, J.-X., Mak, K.F. & Law, K. Theory of Valley Polarized Quantum Anomalous Hall State in Moir\'e MoTe $ _2 $/WSe $ _2 $ Heterobilayers. *arXiv preprint arXiv:2106.13991* (2021).
94. Rademaker, L. Spin-Orbit Coupling in Transition Metal Dichalcogenide Heterobilayer Flat Bands. *arXiv:2111.06208* (2021).
95. Wu, F., Lovorn, T. & MacDonald, A.H. Topological Exciton Bands in Moir\'e Heterojunctions. *Physical Review Letters* **118**, 147401 (2017).
96. Yu, H., Liu, G.-B., Tang, J., Xu, X. & Yao, W. Moiré excitons: From programmable quantum emitter arrays to spin-orbit–coupled artificial lattices. *Science Advances* **3**, e1701696.
97. Ruiz-Tijerina, D.A. & Fal'ko, V.I. Interlayer hybridization and moir\'e superlattice minibands for electrons and excitons in heterobilayers of transition-metal dichalcogenides. *Physical Review B* **99**, 125424 (2019).
98. Shimazaki, Y., Kuhlenkamp, C., Schwartz, I., Smoleński, T., Watanabe, K., Taniguchi, T., Kroner, M., Schmidt, R., Knap, M. & Imamoğlu, A. Optical Signatures of Periodic Charge Distribution in a Mott-like Correlated Insulator State. *Physical Review X* **11**, 021027 (2021).
99. Wilson, N.P., Yao, W., Shan, J. & Xu, X. Excitons and emergent quantum phenomena in stacked 2D semiconductors. *Nature* **599**, 383-392 (2021).
100. Tang, Y., Gu, J., Liu, S., Watanabe, K., Taniguchi, T., Hone, J., Mak, K.F. & Shan, J. Tuning layer-hybridized moiré excitons by the quantum-confined Stark effect. *Nature Nanotechnology* **16**, 52-57 (2021).
101. Zhang, L., Wu, F., Hou, S., Zhang, Z., Chou, Y.-H., Watanabe, K., Taniguchi, T., Forrest, S.R. & Deng, H. Van der Waals heterostructure polaritons with moiré-induced nonlinearity. *Nature* **591**, 61-65 (2021).
102. Liu, E., Barré, E., van Baren, J., Wilson, M., Taniguchi, T., Watanabe, K., Cui, Y.-T., Gabor, N.M., Heinz, T.F., Chang, Y.-C. & Lui, C.H. Signatures of moiré trions in WSe2/MoSe2 heterobilayers. *Nature* **594**, 46-50 (2021).
103. Wang, X., Zhu, J., Seyler, K.L., Rivera, P., Zheng, H., Wang, Y., He, M., Taniguchi, T., Watanabe, K., Yan, J., Mandrus, D.G., Gamelin, D.R., Yao, W. & Xu, X. Moiré trions in MoSe2/WSe2 heterobilayers. *Nature Nanotechnology* **16**, 1208-1213 (2021).
104. Brotons-Gisbert, M., Baek, H., Campbell, A., Watanabe, K., Taniguchi, T. & Gerardot, B.D. Moir\'e-Trapped Interlayer Trions in a Charge-Tunable ${\mathrm{WSe}}_{2}/{\mathrm{MoSe}}_{2}$ Heterobilayer. *Physical Review X* **11**, 031033 (2021).
105. Marcellina, E., Liu, X., Hu, Z., Fieramosca, A., Huang, Y., Du, W., Liu, S., Zhao, J., Watanabe, K., Taniguchi, T. & Xiong, Q. Evidence for Moiré Trions in Twisted MoSe2 Homobilayers. *Nano Letters* **21**, 4461-4468 (2021).
106. Gu, J., Ma, L., Liu, S., Watanabe, K., Taniguchi, T., Hone, J.C., Shan, J. & Mak, K.F. Dipolar excitonic insulator in a moire lattice. *arXiv preprint arXiv:2108.06588* (2021).
107. Zuocheng Zhang, E.C.R., Danqing Wang, Wenyu Zhao, Shaoxin Wang, Mohammed Sayyad, Kentaro Yumigeta, Kenji Watanabe, Takashi Taniguchi, Sefaattin Tongay, Michael Crommie, Alex Zettl, Michael P. Zaletel, Feng Wang.

Correlated interlayer exciton insulator in double layers of monolayer WSe2 and moiré WS2/WSe2. *arXiv:2108.07131* (2021).
108. Bloch, I., Dalibard, J. & Nascimbène, S. Quantum simulations with ultracold quantum gases. *Nature Physics* **8**, 267-276 (2012).
109. Dutta, O., Gajda, M., Hauke, P., Lewenstein, M., Lühmann, D.-S., Malomed, B.A., Sowiński, T. & Zakrzewski, J. Non-standard Hubbard models in optical lattices: a review. *Reports on Progress in Physics* **78**, 066001 (2015).
110. Xie, M. & MacDonald, A.H. Electrical Reservoirs for Bilayer Excitons. *Physical Review Letters* **121**, 067702 (2018).
111. Ma, L., Nguyen, P.X., Wang, Z., Zeng, Y., Watanabe, K., Taniguchi, T., MacDonald, A.H., Mak, K.F. & Shan, J. Strongly correlated excitonic insulator in atomic double layers. *Nature* **598**, 585-589 (2021).
112. Zeng, Y. & MacDonald, A.H. Electrically controlled two-dimensional electron-hole fluids. *Physical Review B* **102**, 085154 (2020).
113. Eisenstein, J.P. & MacDonald, A.H. Bose–Einstein condensation of excitons in bilayer electron systems. *Nature* **432**, 691-694 (2004).
114. Ajesh Kumar, N.C.H., Allan H. MacDonald, Andrew C. Potter. Gate-tunable heavy fermion quantum criticality in a moiré Kondo lattice. *arXiv:2110.11962* (2021).
115. Dalal, A. & Ruhman, J. Orbitally selective Mott phase in electron-doped twisted transition metal-dichalcogenides: A possible realization of the Kondo lattice model. *Physical Review Research* **3**, 043173 (2021).
116. Ya-Hui Zhang, A.V. Electrical detection of spin liquids in double moiré layers. *arXiv:2005.12925* (2020).
117. Xia, F., Wang, H., Hwang, J.C.M., Neto, A.H.C. & Yang, L. Black phosphorus and its isoelectronic materials. *Nature Reviews Physics* **1**, 306-317 (2019).
118. Chaves, A., Azadani, J.G., Alsalman, H., da Costa, D.R., Frisenda, R., Chaves, A.J., Song, S.H., Kim, Y.D., He, D., Zhou, J., Castellanos-Gomez, A., Peeters, F.M., Liu, Z., Hinkle, C.L., Oh, S.-H., Ye, P.D., Koester, S.J., Lee, Y.H., Avouris, P., Wang, X. & Low, T. Bandgap engineering of two-dimensional semiconductor materials. *npj 2D Materials and Applications* **4**, 29 (2020).
119. McGuire, M.A. Crystal and Magnetic Structures in Layered, Transition Metal Dihalides and Trihalides. *Crystals* **7** (2017).
120. Mak, K.F., Shan, J. & Ralph, D.C. Probing and controlling magnetic states in 2D layered magnetic materials. *Nature Reviews Physics* **1**, 646-661 (2019).
121. Hejazi, K., Luo, Z.-X. & Balents, L. Noncollinear phases in moiré magnets. *Proceedings of the National Academy of Sciences* **117**, 10721 (2020).
122. Tong, Q., Liu, F., Xiao, J. & Yao, W. Skyrmions in the Moiré of van der Waals 2D Magnets. *Nano Letters* **18**, 7194-7199 (2018).
123. Akram, M., LaBollita, H., Dey, D., Kapeghian, J., Erten, O. & Botana, A.S. Moiré Skyrmions and Chiral Magnetic Phases in Twisted CrX3 (X = I, Br, and Cl) Bilayers. *Nano Letters* **21**, 6633-6639 (2021).
124. Wang, C., Gao, Y., Lv, H., Xu, X. & Xiao, D. Stacking Domain Wall Magnons in Twisted van der Waals Magnets. *Physical Review Letters* **125**, 247201 (2020).
125. Xu, Y., Ray, A., Shao, Y.-T., Jiang, S., Lee, K., Weber, D., Goldberger, J.E., Watanabe, K., Taniguchi, T., Muller, D.A., Mak, K.F. & Shan, J. Coexisting

ferromagnetic–antiferromagnetic state in twisted bilayer CrI3. *Nature Nanotechnology* (2021).
126. Xie, H., Luo, X., Ye, G., Ye, Z., Ge, H., Sung, S.H., Rennich, E., Yan, S., Fu, Y., Tian, S., Lei, H., Hovden, R., Sun, K., He, R. & Zhao, L. Twist engineering of the two-dimensional magnetism in double bilayer chromium triiodide homostructures. *Nature Physics* (2021).
127. Song, T., Sun, Q.-C., Anderson, E., Wang, C., Qian, J., Taniguchi, T., Watanabe, K., McGuire Michael, A., Stöhr, R., Xiao, D., Cao, T., Wrachtrup, J. & Xu, X. Direct visualization of magnetic domains and moiré magnetism in twisted 2D magnets. *Science* **374**, 1140-1144 (2021).
128. Edelberg, D., Rhodes, D., Kerelsky, A., Kim, B., Wang, J., Zangiabadi, A., Kim, C., Abhinandan, A., Ardelean, J., Scully, M., Scullion, D., Embon, L., Zu, R., Santos, E.J.G., Balicas, L., Marianetti, C., Barmak, K., Zhu, X., Hone, J. & Pasupathy, A.N. Approaching the Intrinsic Limit in Transition Metal Diselenides via Point Defect Control. *Nano Letters* **19**, 4371-4379 (2019).